ATLAS NOTE

ATLAS-CONF-2011-138

August 31, 2011

Search for Charged Higgs Bosons in the τ+jets Final State in $t\bar{t}$ Decays with 1.03 fb^{-1} of pp Collision Data Recorded at $\sqrt{s} = 7$ TeV with the ATLAS Experiment

The ATLAS Collaboration

Abstract

This note presents the results of a search for charged Higgs bosons, $H^{\pm}$, in 1.03 fb^{-1} of proton-proton collision data recorded at $\sqrt{s} = 7$ TeV with the ATLAS experiment at the LHC using the τ+jets channel in $t\bar{t}$ decays with a hadronically decaying τ lepton in the final state. The data agree with the Standard Model expectation leading to a limit on the product of branching ratios BR($t \to bH^{\pm}$)$\times$ BR($H^{\pm} \to \tau\nu$) of 0.03 – 0.10 for $H^{\pm}$ masses in the range 90 GeV $< m_{H^{\pm}} <$ 160 GeV. In the context of the Minimal Supersymmetric Standard Model values of $\tan\beta$ larger than 22 – 30 are excluded in the mass range 90 GeV $< m_{H^{\pm}} <$ 140 GeV.

1 Introduction

The charged Higgs boson is predicted by many non-minimal Higgs scenarios [1, 2], such as models containing Higgs triplets and Two-Higgs-Doublet Models (2HDM) [3]. The observation of charged Higgs bosons[1], $H^{\pm}$, would indicate physics beyond the Standard Model (SM). The analysis in this note considers the type II-2HDM [3], which is also the Higgs sector of the Minimal Supersymmetric Standard Model (MSSM) [4]. For charged Higgs boson masses, m_{H^+}, smaller than the top quark mass, m_t, the dominant production mode at the LHC for H^+ is through top quark decay via $t \to H^+ b$. The dominant source of top quarks at the LHC is through $t\bar{t}$ production; the cross section for charged Higgs boson production from top quark decays in single-top events is much smaller and not considered here. For $\tan\beta > 3$, where $\tan\beta$ is the ratio of the vacuum expectation values of the two Higgs doublets, charged Higgs bosons decay mainly via $H^+ \to \tau\nu$ [5]. Recent limits on light charged Higgs boson production come from the Tevatron [6], where the observed upper limit on $\mathrm{BR}(t \to H^+ b)$ assuming $\mathrm{BR}(H^+ \to \tau^+\nu) = 1$ is 0.17 for $m_{H^+} = 120$ GeV. Direct searches at LEP [7] give a lower limit of $m_{H^+} \simeq 90$ GeV for $\mathrm{BR}(H^+ \to \tau^+\nu) = 1$. Preliminary results for charged Higgs boson searches in top quark decays have recently been made public by the CMS experiment [8].

This note describes the search for charged Higgs bosons in $t\bar{t}$ events in the topology shown in Fig. 1, for the case where both the τ lepton and the W decay hadronically (τ+jets channel).

The H^+ search uses proton-proton collision data collected with the ATLAS experiment [9] at the LHC at a center-of-mass energy of $\sqrt{s} = 7$ TeV in 2011. The total integrated luminosity amounts to 1.03 fb^{-1} .

The background processes that enter these searches include the production of $t\bar{t}$, single-top, W+jets, Z/γ^*+jets, and multi-jet events where there is either a true τ lepton, or another object misidentified as a hadronically decaying τ. In this note, all significant backgrounds, i.e. events with correctly identified hadronically decaying τ leptons (hereafter referred to as τ jets), or with jets or electrons misreconstructed as τ jets, are estimated using data-driven methods.

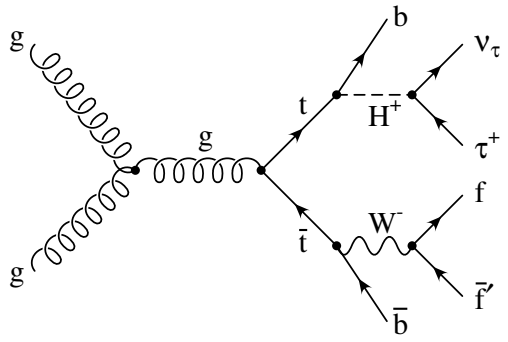

Figure 1: Example for a leading-order Feynman diagram for the production of a charged Higgs boson through gluon fusion in $t\bar{t}$ decays.

2 Physics processes and their cross sections

All relevant backgrounds are estimated using data-driven techniques. However, for backgrounds with intrinsic missing transverse energy and objects misidentified as τ jets, simulation is used to model any aspects not related to the probability of the object to be misidentified as a τ jet. For backgrounds without

[1]Hereafter the charged Higgs bosons will be denoted H^+, with the charge-conjugate H^- always implied.

intrinsic $E_{\mathrm{T}}^{\mathrm{miss}}$ (multi-jet background), simulation is used to subtract the electroweak and $t\bar{t}$ contribution in the control region. Simulation is also used for comparison with the results of the data-driven estimates.

The Monte Carlo (MC) simulation of $t\bar{t}$ and single-top events is based on MC@NLO [10] using HERWIG [11] for the hadronization process and JIMMY [12] for simulating multi-parton interactions. Overlap between $t\bar{t}$ and single-top final states is taken into account [13]. A $t\bar{t}$ production cross section of 165 pb [14] obtained from approximate NNLO calculations [15] is used (both for SM $t\bar{t}$ decays and decays via a charged Higgs boson). The MC@NLO cross sections are used for single-top production. Throughout this note, a top quark mass of 172.5 GeV is assumed.

ALPGEN [16] is used for the generation of W+jets and Z/γ^*+jets events with up to five partons from the hard matrix element, again together with HERWIG/JIMMY. The ALPGEN cross sections are rescaled by a factor 1.20 (W) and 1.25 (Z/γ^*) to match NNLO calculations [17]. The H^+ signal events are generated with PYTHIA [18], using TAUOLA [19] for τ lepton decays and PHOTOS [20] for photon radiation off charged leptons. Event generators are tuned to describe ATLAS data, and the parameter sets AMBT1 [21] and AUET1 [22] are used for this purpose for events hadronized with Pythia, and with HERWIG/JIMMY, respectively.

Table 1: Simulated events used in this study. The W/Z+jets as well as the s- and t-channel single-top events are only simulated for decays involving leptons (ℓ denotes e, μ, or τ), and the cross section given includes this branching ratio. The NLO+NNLL cross section is used for $t\bar{t}$, NLO for single-top, and NNLO for W/Z+jets. The H^+ sample uses $m_{H^+} = 130$ GeV, BR($t \to bH^+$) = 0.1 and BR($H^+ \to \tau^+\nu$) is assumed to be 1.

Process	Generator	Cross section [pb]
$t\bar{t}$ with $\geq 1\ell$	MC@NLO	89.4
single-top (s, t, Wt channel)	MC@NLO	21.4, 1.41, 14.6
$W \to \ell\nu$+jets	ALPGEN	$3.1 \cdot 10^4$
$Z/\gamma^* \to \ell\ell$+jets	ALPGEN	$3.2 \cdot 10^3$
$t\bar{t} \to bH^{\pm}bW$ with $H^{\pm} \to \tau\nu$	PYTHIA	29.6

All events are propagated through a detailed GEANT4 [23, 24] simulation of the ATLAS detector and reconstructed by the same algorithms as the data. Cross sections and simulated event samples are summarized in Table 1.

3 Object reconstruction

A description of the ATLAS detector can be found elsewhere [9]. In this section, the criteria used to identify and reconstruct physics objects such as leptons or jets are described.

Data quality: For both the H^+ event selection and the data-driven background estimates, the following requirements are applied [25]: The sub-detectors relevant to the analyses have been operational, the LHC delivered stable beams, and there are no jets in the event consistent with coming from instrumental effects such as coherent noise in the electromagnetic calorimeter, or non-collision backgrounds. To further reject non-collision backgrounds, only events with a reconstructed primary vertex with at least five associated tracks are considered.

Jets: Jets are reconstructed with the anti-k_t algorithm [26, 27] with a size parameter value of $R = 0.4$. The jet finder uses three-dimensional noise-suppressed clusters [28] in the calorimeter, reconstructed at

the electromagnetic (EM) energy scale. Jets are then calibrated to the hadronic energy scale with Monte-Carlo-based correction factors which depend on their transverse momentum (p_{T}) and pseudorapidity (η). The jet energy scale uncertainty is estimated to be (2.5 − 14)%, depending on p_{T} and η, with methods described in Ref. [29] but based on a larger data set. Jets considered in this analysis are required to have $p_{\mathrm{T}} > 20$ GeV and $|\eta| < 2.5$.

***b* jets:** To identify jets initiated by b quarks, a combination of a 3D-impact-parameter-based discriminant and a secondary-vertex-tagger [30] with an identification efficiency of about 60% for b jets with $p_{\mathrm{T}} > 20$ GeV in $t\bar{t}$ events is applied.

τ jets: For the reconstruction of τ jets, all anti-k_t jets in the calorimeter with $E_{\mathrm{T}} > 10$ GeV are considered as τ candidates [31]. A dedicated algorithm is used to reject electrons (called tight electron veto). Only candidates with 1 or 3 associated tracks reconstructed in the inner detector are considered. Hadronic τ decays are identified using a likelihood quality criterion (corresponding to an efficiency of about 30% for τ leptons with $p_{\mathrm{T}} > 20$ GeV in $Z \to \tau\tau$ events, and a rejection factor of about 100-1000 for quark- and gluon-initiated jets, depending on p_{T}, η, and the number of associated tracks). For this analysis, they are required to have a visible $p_{\mathrm{T}} > 20$ GeV and to be within $|\eta| < 2.3$. In some control regions, a loose τ identification is used instead; this corresponds to an efficiency of 60%, and a jet rejection of about 10, depending on p_{T} and η.

Electrons: Electrons are reconstructed by matching clustered energy deposits in the electromagnetic calorimeter to tracks reconstructed in the inner detector [32]. They are required to meet quality requirements based on the expected shower shape of electrons [33]. Electrons are required to have $E_{\mathrm{T}} > 20$ GeV, and be isolated (defined by requiring less than 3.5 GeV of transverse energy – after corrections for pile-up and leakage – in a cone of $\Delta R = 0.2$ around the electron[2], excluding the electron itself). Electrons are required to be in the fiducial volume of the detector, $|\eta| < 2.47$. Electrons in the transition region $1.37 < |\eta| < 1.52$ are excluded.

Muons: Muon candidates are required to have a match of an inner detector track with a track reconstructed in the muon spectrometer [34]. Candidates are required to have $p_{\mathrm{T}} > 10$ GeV and $|\eta| < 2.5$. Only isolated muons are accepted by requiring that in a cone of $\Delta R = 0.3$ around the muon (excluding the muon itself), both the energy deposited in the calorimeters and the momentum of all inner detector tracks total less than 4 GeV of transverse energy.

Missing transverse energy, transverse energy sum: The reconstructed missing transverse energy, $E_{\mathrm{T}}^{\mathrm{miss}}$, is based on the energy deposited in the calorimeter and the momentum of tracks identified as associated to muons. Only noise-suppressed clusters of cells are used, and corrections for unclustered cells are applied. The contribution of the calorimeter cells is calibrated differently depending on which object they are associated to. For all jets, the same hadronic calibration scheme as for jet reconstruction is used while electrons are calibrated at the electromagnetic energy scale [35].

The transverse energy sum, $\sum E_{\mathrm{T}}$, is defined as the sum of the transverse energy of all the objects which have been reconstructed as detailed in this section, including missing transverse energy.

[2] $\Delta R = \sqrt{(\Delta\eta)^2 + (\Delta\phi)^2}$, where $\Delta\eta$ is the difference in pseudorapitidy of the two objects in question, and $\Delta\phi$ the difference of their azimuthal angles.

Overlap removal: When candidates selected using the above criteria overlap geometrically with one another (within $\Delta R < 0.2$), this conflict is resolved by only selecting one candidate in the following order of priority: muon, electron, τ jet, or jet.

General systematic uncertainties The main detector-related systematic uncertainties are listed in Table 2. These are mostly related to identification efficiencies and the energy/momentum resolution and scale of the physics objects described above. Uncertainties on trigger efficiency, luminosity, cross sections and acceptance are also listed.

To assess the impact of most sources of systematic uncertainty on the result of the analysis, selection cuts for each analysis are re-applied after shifting a particular parameter by its ± 1 standard deviation uncertainty. The luminosity and the trigger uncertainty with respect to the offline efficiency serve directly as scale factors on the event yield.

Table 2: Systematic uncertainties. Uncertainties on the $t\bar{t}$ cross section include variations of the parton density functions (pdf) and of the factorization and renormalisation scale. A scale factor is the ratio of efficiencies in data and simulation, and is here denoted as "SF". The difference in acceptance for $t\bar{t}$ events at LO and NLO is used as systematic uncertainty on the signal acceptance.

Quantity	Uncertainty
Luminosity [36]	±3.7%
Jet energy resolution (JER)	$\pm(10-30)$%, depending on p_{T} and η
Jet energy scale (JES)	$\pm(2.5-14)$%, depending on p_{T} and η
$E_{\mathrm{T}}^{\mathrm{miss}}$	Uncertainty due to scale/resolution uncertainties (e.g. JES); additional 10% of pile-up-related uncertainty
b-tagging efficiency SF unc.	$\pm(0.05-0.15)$, depending on p_{T} and η
b-tagging mistag rate	$\pm(0.16-0.39)$, depending on p_{T} and η
b jets JES uncertainty	an additional ±2.5% on top of the standard JES
τ identification efficiency	$\pm(8.5-9.9)$%, depending on p_{T}
τ energy scale	$\pm(4.5-6.5)$%, depending on p_{T}, η, number of associated tracks
τ electron mis-id correction factors	$\pm(23-100)$%, depending on η; for one-prong only
τ+$E_{\mathrm{T}}^{\mathrm{miss}}$ trigger	±9%
e reco. efficiency SF	$\pm(0.7-1.8)$%, depending on η
e identification efficiency SF	$\pm(2.2-3.8)$%, depending on E_{T} and η
e energy scale	$\pm(0.3-1.8)$%, depending on p_{T} and η
e energy resolution	$\pm(0.5-2.4)$% (additional constant term), depending on p_{T} and η
μ reco. efficiency SF	$\pm(0.25-0.55)$%, depending on the data-taking period
μ momentum scale and resolution	$\pm(0.4-0.7)$%, depending on η
Initial/final state radiation modelling	-16% / +19% ($t\bar{t}$ signal and background)
Acceptance	± 4% (background), ± 10% (signal)
$t\bar{t}$ cross section	165^{+4}_{-9}(scale) $^{+7}_{-7}$(pdf) pb

4 Event selection

This study describes the search for a charged Higgs boson in the topology

$$t\bar{t} \to [H^+b]\,[W^-\bar{b}] \to [(\tau^+_{had}+\nu)b]\,[(q\bar{q}')\bar{b}], \tag{1}$$

where both the W boson and the τ lepton decay hadronically. This topology has the advantage that the W boson can be fully reconstructed, the H^+ candidate can be reconstructed in the transverse plane, and

the branching ratio of the W boson decay to quarks is larger than that to leptons; but it needs to be distinguished from a large multi-jet background.

The following selection cuts are applied, based on the reconstructed physics objects described in Section 3:

1. Event preselection:
   (a) Data quality cuts.
   (b) $E_{\mathrm{T}}^{\mathrm{miss}}$ plus tau trigger [37, 38], with a threshold of 29 GeV on the τ object, of 35 GeV on $E_{\mathrm{T}}^{\mathrm{miss}}$, and no muon corrections on $E_{\mathrm{T}}^{\mathrm{miss}}$. The signal efficiency is about 70%, depending on m_{H^+}.
   (c) At least 4 jets (excluding τ jets) with $p_{\mathrm{T}} > 20$ GeV and $|\eta| < 2.5$.
2. A τ jet with $p_{\mathrm{T}}^{\tau} > 35$ GeV within $|\eta| < 2.3$ is required. This τ jet must be matched to the τ trigger object within $\Delta R < 0.1$. Events with a second identified τ jet with $p_{\mathrm{T}}^{\tau} > 20$ GeV are vetoed.
3. Events are vetoed if any identified electrons ($E_{\mathrm{T}} > 20$ GeV) or muons ($p_{\mathrm{T}} > 10$ GeV) are present.
4. The missing transverse energy $E_{\mathrm{T}}^{\mathrm{miss}}$ is required to be larger than 40 GeV.
5. Events with large reconstructed $E_{\mathrm{T}}^{\mathrm{miss}}$ due to the limited resolution of the energy measurement are rejected with a cut on the ratio $\frac{E_{\mathrm{T}}^{\mathrm{miss}}}{0.5 \cdot \sqrt{\sum E_{\mathrm{T}}}} > 8$ GeV$^{1/2}$, using the $\sum E_{\mathrm{T}}$ definition described in Section 3. Considering the minimum $\sum E_{\mathrm{T}}$ required to pass all other selection cuts, this also corresponds to raising the cut on $E_{\mathrm{T}}^{\mathrm{miss}}$ to about 50 GeV.
6. At least one b-tagged jet is required.
7. Topologies consistent with a top decay are identified by requiring that the qqb candidate with the highest p_{T}^{qqb} value must satisfy $m(qqb) \in [120, 240]$ GeV.

For events passing the above selection cuts the transverse mass, m_{T}, is defined as

$$m_{\mathrm{T}} = \sqrt{2 p_{\mathrm{T}}^{\tau} E_{\mathrm{T}}^{\mathrm{miss}} (1 - \cos \Delta\phi)}, \tag{2}$$

where $\Delta\phi$ is the azimuthal angle between the τ jet and the missing energy direction. This final discriminating variable is related to the W boson mass in the $W \to \tau\nu$ background case, and the H^+ mass for the signal hypothesis.

At the end of the selection cut flow, after applying data-driven methods as detailed in the sections that follow, 37 ± 7 background events are expected for $m_{\mathrm{T}} > 40$ GeV. Of those, 21 ± 5 events are expected with a correctly identified τ jet; about 2 events each for the case where an electron or a jet have been misidentified as a hadronically decaying τ lepton in a $t\bar{t}$ or electroweak background process. The multi-jet contribution is expected to be 12 ± 5 events. A potential signal yield depends on the charged Higgs boson mass and the branching ratio $t \to bH^+$; for example, 70 events are expected for $m_{H^+} = 130$ GeV and BR($t \to bH^+$)=0.1.

5 Data-driven background estimation

The main source of background events to charged Higgs boson searches at the LHC are those coming from production processes such as $t\bar{t}$, multi-jet, single top-quark, and W+jets, in this order of relevance. The individual contributions from these backgrounds are determined in a data-driven way. They can

be divided into two categories: backgrounds with intrinsic $E_{\mathrm{T}}^{\mathrm{miss}}$ from W decays, and backgrounds with $E_{\mathrm{T}}^{\mathrm{miss}}$ caused by detector effects (multi-jet events). For the first category, the contribution from events in which electrons or jets are misidentified as τ jets are predicted using appropriate control samples while events with correctly identified τ jets are studied with the embedding method. The multi-jet background can be estimated using the shape of its $E_{\mathrm{T}}^{\mathrm{miss}}$ distribution in a suitable control region.

5.1 Methods based on measuring misidentification probabilities

The background from events where an electron or a jet is misidentified as a hadronically decaying τ lepton is estimated in a data-driven procedure from suitable control samples. The probability for an electron or jet to be misidentified as a τ jet is defined as

$$\text{misidentification probability} = \frac{\text{number of } \tau \text{ candidates passing event selection, } \tau \text{ ID and electron veto}}{\text{number of } \tau \text{ candidates passing event selection}}. \tag{3}$$

5.1.1 Electron-to-τ misidentification probability with a tag-and-probe method

The Method A tag-and-probe method on Z/γ^* events in collision data is used to measure the misidentification probability of electrons. The result is compared to simulation, and the ratio of the misidentification probability as measured in data to that determined in simulation is called a scale factor. This factor is then used to correct the description of the electron-to-τ misidentification probability in simulation. The method used is identical to that described in [39] though based on a larger data set. The process $Z/\gamma^* \rightarrow ee$ allows the selection of a clean sample of electrons from data. An electron trigger with a threshold on the electron E_{T} of 20 GeV is used. The tag electron is required to have a $p_{\mathrm{T}} > 30$ GeV and to be located in the central region ($|\eta| < 2.47$) of the detector (but outside the transition region between the barrel and the end-cap, $1.37 < |\eta| < 1.52$). It must be isolated (the sum of the momenta of tracks in a cone of $\Delta R = 0.4$ around the electron is required to be less than 6% of the electron momentum) and must pass tight electron identification criteria [33]. Furthermore, a match within $\Delta R = 0.1$ to the trigger electron is required. The probe electron is considered for further analysis if it is reconstructed as a τ jet candidate with $p_{\mathrm{T}} > 20$ GeV with exactly one associated track. The probability of electrons to be misidentified as 3-track τ jets is negligible. The pair with the highest scalar E_{T} sum is chosen from all possible e-τ pairs that are separated by $\Delta R > 0.4$. Additionally, the tag and the probe objects are required to have opposite electric charges. Events with $E_{\mathrm{T}}^{\mathrm{miss}} > 20$ GeV are discarded to reduce the background contamination from $W \rightarrow e\nu$ decays, and the invariant mass of the e-τ pair is required to be between 80 and 100 GeV.

The selected probe sample of τ jet candidates then contains electrons originating from Z bosons with a purity (estimated from simulation) of about 99%. The main backgrounds are multi-jet events, $W \rightarrow e\nu$, and $Z/\gamma^* \rightarrow \tau\tau$, in that order. The multi-jet background is estimated using a two-dimensional sideband subtraction method [39], the electroweak backgrounds using simulation.

Results The misidentification probabilities (as defined in Eq. 3) are extracted for the τ candidates which pass the τ selection (including overlap removal with electron candidates) and the electron veto criteria as used in the H^+ selection. In the denominator, the probe objects are not required to pass the τ jet identification, whereas the numerator contains the number of events with the probe objects both passing the identification and not being discarded by the electron veto. The results for the scale factor and misidentification probability are shown in Table 3 for the different calorimeter regions. Only the scale factors are used in the following. No significant dependence of the scale factor on the p_{T} of the τ lepton candidate is observed.

Application of the method to estimate the $e \to \tau$ misidentification background The misidentification probability from this study is applied by scaling simulated events in which the selected reconstructed τ jet originates from a true electron. The scale factor used is given by the ratio of the misidentification probability in data to that in Monte Carlo.

Table 3: Scale factors and measured $e \to \tau$ misidentification probabilities for τ candidates with $E_{\mathrm{T}} > 20$ GeV in the barrel ($0<|\eta|< 1.37$), transition ($1.37<|\eta|< 1.52$) and end-cap ($1.52 <|\eta|< 2.5$) regions passing the τ identification and a tight electron veto, for a τ identification efficiency of about 30%. The scale factors are given with statistical and systematic uncertainties combined.

Region	Scale factor	Misidentification probability (data)
$0 < \lvert\eta\rvert < 1.37$	1.1 ± 0.3	0.0028 ± 0.0006
$1.37 < \lvert\eta\rvert < 1.52$	1.0 ± 1.0	0.0005 ± 0.0004
$1.52 < \lvert\eta\rvert < 2.5$	1.6 ± 0.5	0.009 ± 0.003

Systematic uncertainties Five main sources of systematic uncertainties on the electron-τ jet misidentification probability are studied. The systematic uncertainty due to the subtraction of multi-jet and electroweak backgrounds is at the level of only 1%, but can reach up to 25% in the transition region. Ideally, the measurement should be independent of the tag selection. To test any potential correlation, this selection has been varied (using medium electron identification criteria instead of tight ones in order to study the bias of only selecting very well-reconstructed tag electrons), leading to an estimate of a systematic uncertainty of 10%. Other systematic uncertainties are negligible in comparison. The choice of the mass window size around m_Z applied to the tag-and-probe objects which could result in a bias by only studying objects with well-reconstructed momentum and the uncertainty of the electron energy scale (via the cut on the tag electron energy) only give a small contribution. The total uncertainties on the scale factors (combining the statistical and systematic uncertainties of the measurement) are 24% in the barrel, 29% in the end-caps, and 100% in the transition region. Except for the end-cap, they are dominated by the statistical uncertainties.

In total, the expected contribution of events with electrons misidentified as τ jets in the signal region is about 2 events which is about 5% of the expected background. Thus reducing the relatively large uncertainties would only lead to a minor improvement of the H^+ sensitivity.

5.1.2 Jet-to-τ misidentification probability from photon+jets

To study the probability for jets to be misidentified as hadronically decaying τ leptons, a γ-jet control sample is used. Like jets from the hard process in the dominant H^+ background $t\bar{t}$, jets in this control sample originate predominantly from quarks as opposed to gluons. A measurement of the probability for a jet to be misidentified as a hadronically decaying τ lepton is performed using 1.03 fb^{-1} of data and is used to predict the yield of jet-to-τ misidentification events from the most important SM backgrounds with intrinsic $E_{\mathrm{T}}^{\mathrm{miss}}$. The main difference between $t\bar{t}$ and γ-jet events is the different fraction of b jets which is smaller in γ-jet events. However, the probability for a b jet to be misidentified as a τ jet is smaller than the corresponding probability for a light-quark jet: The average track multiplicity of b jets is higher, and variables which measure the mass of the τ candidate allow a good discrimination. Hence using the γ-jet misidentification probability leads to a higher background estimate and is thus conservative.

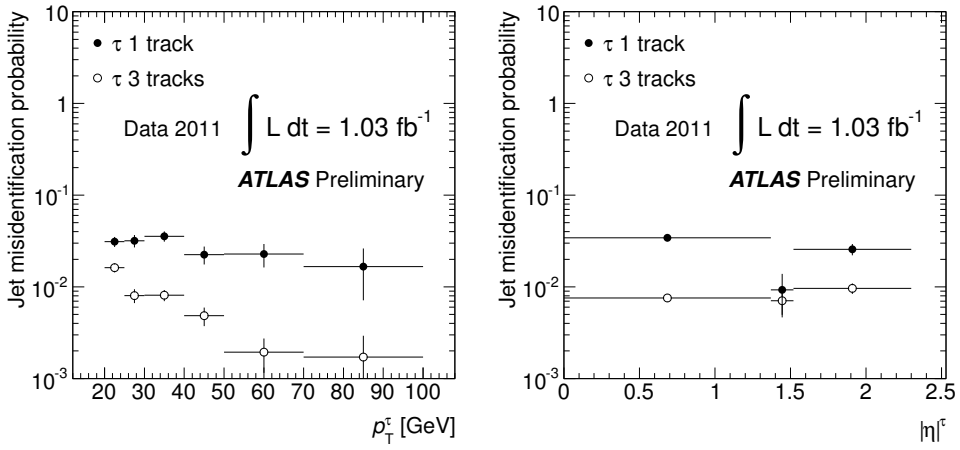

Figure 2: Jet→ τ misidentification probability measured from γ-jet events for jets with 1 or 3 associated tracks as a function of p_{T} and η. The error bars indicate the size of the statistical uncertainties.

The Method Events are required to pass a single-photon trigger (with an E_{T} threshold of 15, 20 or 40 GeV). The photon candidate must be isolated (less than 6 GeV of E_{T} deposited in a $\Delta R = 0.2$ cone around the photon), is required to match a trigger object, pass the photon selection [40], and have either zero or two associated tracks to include photon conversions. The photon candidate must have $|\eta| < 2.37$, not be located in the transition region, and must have a transverse energy of at least 15 GeV. The selected γ-jet sample consists of events with one photon candidate and a jet with $p_{\mathrm{T}} \geq 20$ GeV, separated in ϕ by at least 2.84 radians. The difference in transverse energy between the jet and the photon must be less than half of the total transverse energy of the photon. Any additional jets are required to have less than 20% of the photon transverse energy.

The misidentification probability is measured as a function of both p_{T} and η. The denominator of the calculated misidentification probability is the number of events with a τ candidate (i.e. no τ ID applied) with p_{T} greater than 20 GeV and $|\eta| < 2.3$, which passes an electron veto. The misidentification probability is evaluated separately for the case of candidates with 1 or 3 associated tracks. Among all jets with $E_{\mathrm{T}} > 20$ GeV and $|\eta| < 2.3$, the fraction of light-quark jets which are considered as such τ candidates is about 27%. The numerator in the calculated misidentification probability consists of events with objects which pass the full τ identification. They must not be within $\Delta R = 0.2$ of any e or μ. The measured misidentification probabilities are shown in Fig. 2.

Systematic uncertainties The dominant systematic uncertainties on the misidentification probability are (the ranges given on each systematic uncertainty show the variation with the p_{T} and η of the τ candidate):

- Contamination of the control sample with true τ jets from $Z \to \tau\tau$ and $W \to \tau\nu$ events, evaluated using simulation: $(1 - 3)\%$.

- Contamination of the control sample with multi-jet events which have a larger gluon-initiated jet fraction than γ-jet events. The associated systematic uncertainty is evaluated by modifying the photon ID requirements, in particular loosening the photon isolation which increases the impurity from multi-jet events in the control sample: $(5 - 9)\%$.

- Contamination of the control sample by three-jet events. The associated systematic uncertainty is evaluated by varying the selection cuts (vetoing events with additional jets with less than 0.1 of the

photon momentum), and by splitting the control sample in a part which fulfills even tighter requirements and one which does not, and then taking the variation of the misidentification probability due to these changes as the uncertainty: $(11 - 17)\%$.

- The measurement of the misidentification probability on the probe object is assumed to be uncorrelated from the selection of the tag object. To evaluate uncertainties from a violation of this assumption, correlations between the tag and the probe objects are studied by changing the requirements on the tag object (requiring a photon with a looser quality criterion) and studying the impact on the measurement of the misidentification probability on the probe object: $(7 - 14)\%$.

Additionally, the statistical uncertainty of the measurement of the misidentification probability enters as uncertainty on any application of the misidentification probability. The total systematic uncertainty is about $(15 - 24)\%$, depending on p_{T} and η. The systematic uncertainties on the misidentification probability are propagated into the background prediction for the baseline selection and enter the statistical evaluation as shape uncertainties.

Application to estimate the jet$\rightarrow \tau$ misidentification background To predict the background in H^+ searches, the measured jet$\rightarrow \tau$ misidentification probability is applied to simulated $t\bar{t}$, single-top, and W+jets events. These events are required to pass the full event selection except for the τ identification. For these events, τ candidates fulfilling the same requirements as in the misidentification probability definition which do not overlap with a true τ lepton are identified. Out of the remaining τ candidates, each one is considered to be potentially misidentified as a τ jet separately. The identified jet that corresponds to the τ candidate is removed from the event, affecting the number of reconstructed jets, the $E_{\mathrm{T}}^{\mathrm{miss}}$ significance of the event, and the number of b-tagged jets. If, after taking this into consideration, the event still passes the selection, then the event is counted as background event with a weight given by the misidentification probability corresponding to the p_{T} and the η of the τ candidate. The predicted number of events from the $t\bar{t}$ sample, together with a comparison to the MC prediction using truth information, is shown in Table 4. All other jet$\rightarrow \tau$ misidentification backgrounds with intrinsic $E_{\mathrm{T}}^{\mathrm{miss}}$ are at least two orders of magnitude smaller than $t\bar{t}$.

Table 4: Application of the misidentification probability obtained from γ-jet events. The numbers shown are the expected number of events in collision data after the H^+ selection. The prediction based on the misidentification probability measurement (statistical and systematic uncertainties), as well as the MC prediction (statistical uncertainties), are given.

Sample	Data-driven prediction [number of events]	MC prediction [number of events]
$t\bar{t}$	$2.8 \pm 1.0(\mathrm{stat}) \pm 0.5(\mathrm{syst})$	$3.8 \pm 0.6(\mathrm{stat})$

5.2 Multi-jet background estimate

As the uncertainties on the multi-jet expectation are large, it is necessary to avoid using any multi-jet simulation to estimate this background. Thus an approach different from estimating the jet$\rightarrow \tau$ misidentification contribution in events with intrinsic $E_{\mathrm{T}}^{\mathrm{miss}}$, as described in the previous section, is chosen.

The Method The multi-jet background is estimated by fitting its $E_{\mathrm{T}}^{\mathrm{miss}}$ shape (and the $E_{\mathrm{T}}^{\mathrm{miss}}$ shape of other backgrounds) to data. In order to study this shape in a data-driven way, a control region is defined

where the τ identification and b-tagging requirements are inverted. The τ candidates must pass a loose τ identification but fail the tight τ identification used in the baseline selection. In addition, the event is required not to contain any b-tagged jets and therefore also the requirement on the qqb mass (selection cut 7) is removed.

Assuming that the shapes of the $E_{\mathrm{T}}^{\mathrm{miss}}$ and m_{T} distributions are the same in the control sample and signal regions (see Fig. 3 for a comparison early in the selection cut flow), the shape of the $E_{\mathrm{T}}^{\mathrm{miss}}$ distribution is used to model the $E_{\mathrm{T}}^{\mathrm{miss}}$ distribution for the multi-jet background (after subtracting the background from other processes). The $E_{\mathrm{T}}^{\mathrm{miss}}$ distribution measured in data (for the baseline selection) is then fitted using two shapes: this multi-jet model, and the sum of other processes (dominated by $t\bar{t}$, W+jets) for which the shape and the relative normalisation are taken from MC simulation. The free parameters in the fit are the overall normalisation (to the one in data) and the multi-jet fraction.

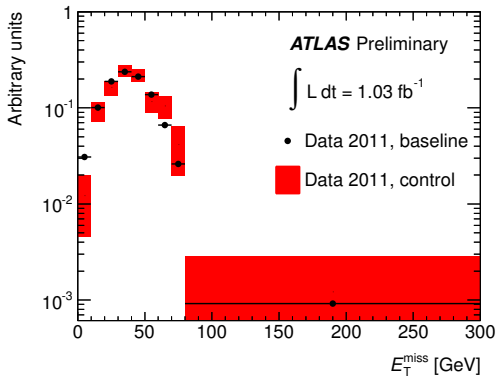

Figure 3: Distribution of $E_{\mathrm{T}}^{\mathrm{miss}}$, after subtracting the expectation from $t\bar{t}$, W+jets, and single-top simulation; compared are the distributions after requirement 3 of the baseline selection as detailed in Section 4, with the exception that in the control region, the τ selection and the b-tagging requirements have been inverted. The shaded area indicates the size of the statistical uncertainties.

Systematic uncertainties The dominant systematic uncertainties are:

- The uncertainty on the assumption that the $E_{\mathrm{T}}^{\mathrm{miss}}$ shape is identical in the signal and control regions. This is studied by varying the number of entries in each bin separately within the maximum differences observed early in the selection cut flow (a factor of 0.5 and 2.0) and redoing the fit. Then, the largest downwards and upwards fluctuations are used as systematic uncertainty. This leads to an uncertainty on the multi-jet fraction of $-13\%/+25\%$.
- The uncertainty on the $t\bar{t}$ and W+jets shapes and relative normalisation from Monte Carlo is dominated by uncertainties on the $t\bar{t}$ cross section. The scaling of the $t\bar{t}$ Monte Carlo is varied according to these uncertainties, leading to an uncertainty on the multi-jet fraction of 2.4%.
- The uncertainty from backgrounds other than $t\bar{t}$ and W+jets in the control region is found to be negligible.

The uncertainty on the multi-jet fraction is dominated by the statistical uncertainty of the data set on which the fit is performed.

Result of the data-driven estimate of the multi-jet background The multi-jet fraction is estimated to be $(23 \pm 10)\%$ using the fit to the $E_{\mathrm{T}}^{\mathrm{miss}}$ distribution shown in Fig. 4. The m_{T} distribution for the same

events is shown in Fig. 5. Except for the multi-jet background, all other processes have W bosons in the final state and their distributions drop off around the W boson mass, as expected. Such behavior is neither expected nor observed for the multi-jet background as resulting shapes are mainly caused by detector effects. To probe the region with large m_{T}, in which a potential H^+ signal resides, it is thus important to suppress the multi-jet background as much as possible.

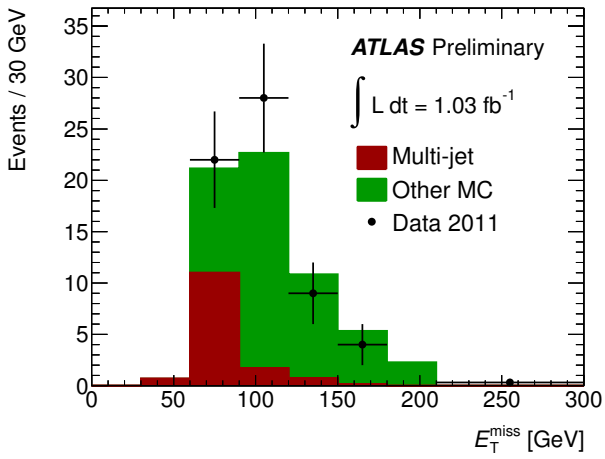

Figure 4: Multi-jet estimate: A fit to the $E_{\mathrm{T}}^{\mathrm{miss}}$ distribution in data after all selection cuts using two shapes (one for the multi-jet model, and one for all other background processes, dominated by $t\bar{t}$ and W+jets) is shown. The multi-jet fraction estimated after all selection cuts is (23 ± 10)%.

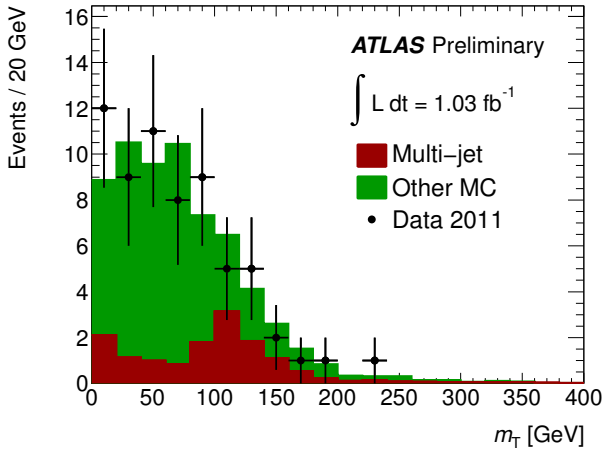

Figure 5: Contribution of multi-jet events to the m_{T} distribution after all cuts of the H^+ selection. The multi-jet fraction is estimated using the fit to the $E_{\mathrm{T}}^{\mathrm{miss}}$ distribution shown in Fig. 4.

5.3 Embedding method

Complementary to the methods based on misidentification probability, an embedding method is used for estimating the background from true τ jets, described below. The method consists of collecting a control sample of $t\bar{t}$, single-top, and W+jets events with a muon in data, and replacing the detector signature of this muon with that of a simulated τ lepton. The reconstruction is re-applied to the new hybrid

events which are then used to estimate the background to the H^+ selection. The advantage is that the whole event (except for the τ jet) is taken directly from data, including the underlying event and pile-up, missing energy, b-quark jets and light-quark jets. The method has been validated in τ+jets events using early ATLAS data [41].

5.3.1 The Method

Control sample selection To select the $t\bar{t}$-like μ + jets control sample from data, the following event selection is used:

- Event triggered by a single muon trigger (p_{T} threshold of 18 GeV),
- data quality cuts as described in Section 3,
- exactly one isolated muon with $p_{\mathrm{T}} > 25$ GeV,
- no isolated electron with $p_{\mathrm{T}} > 20$ GeV,
- at least four jets with $p_{\mathrm{T}} > 20$ GeV in $|\eta| < 2.5$,
- at least one of the jets is b-tagged (nominal efficiency of 65%),
- missing transverse energy $E_{\mathrm{T}}^{\mathrm{miss}} > 30$ GeV,
- scalar sum of energy of reconstructed objects $\sum E_{\mathrm{T}} > 200$ GeV.

This selection is looser than the selection defined in Section 4 in order not to bias the control sample. This also applies to the τ jet which carries the momentum of the selected muon minus the momentum of the neutrino in the τ lepton decay and its p_{T} is required to be larger than 35 GeV in the H^+ selection. The impurity from the background with muons produced in τ decays, and non-isolated muons (dominantly $b\bar{b}$ and $c\bar{c}$ events) is at the level of 10% and biases the shape of embedded events. However, the bias is greatly reduced as these events are much less likely to pass the H^+ selection.

Embedding step After events have been selected, the actual embedding step takes place. The muon in the event is selected and its vertex position and momentum are extracted. The momentum is then rescaled to account for the higher τ lepton mass and fed into TAUOLA to produce the τ lepton decay products and generate final state radiation. The result is propagated through ATLAS detector simulation, followed by reconstruction. In the next step, tracks, calorimeter deposits and segments in the muon spectrometer in the vicinity of the muon are replaced with those of the simulated τ lepton decay products.

Comparison of embedding method versus simulation To test the method, the embedded data events are compared to simulated $t\bar{t}$ events (hereafter referred to as 'reference') in which the τ lepton comes directly from simulation of the whole event, and is not added via the embedding method. To make sure the set of events is comparable, both for the embedded and the reference events, a reconstructed τ candidate which is matched to a true τ lepton is required (this can be performed using embedded events, as the τ part of the event is taken from simulation).

A comparison of distributions of variables relevant to this analysis is shown in Fig. 6. A good agreement is observed within the statistical uncertainties.

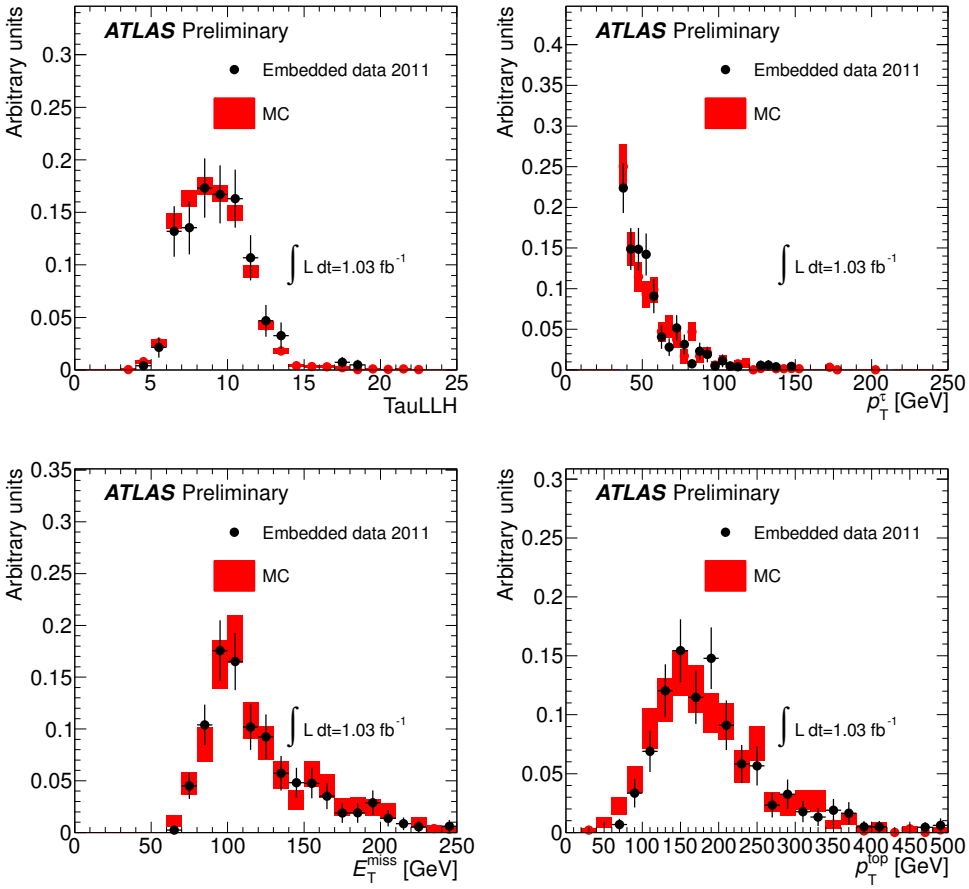

Figure 6: Validation plots for the embedding method used to estimate the background with true τ jets. Embedded data is compared to $t\bar{t}$ simulation after applying the H^+ selection. The τ likelihood (TauLLH), the τ transverse momentum, the missing transverse energy, and the top quark transverse momentum on the $t \to bqq$ side are shown. The plots are normalized to unit area. The shaded area indicates the size of the statistical uncertainties on the MC simulation.

5.3.2 Application to estimate the true-τ background

The contribution of backgrounds with true τ jets to the final m_{T} distribution is estimated from this distribution for embedded events. The normalisation is taken from collision data events in the region $0 - 40$ GeV of this distribution, where any signal contamination would be low for the expected range of sensitivity (BR($t \to bH^+ \approx 5\%$)). Such a contamination is dealt with in the limit-setting process by subtracting the expected signal from the observed data before normalizing the shape to the region $m_{\mathrm{T}} < 40$ GeV. This is done when evaluating the signal+background hypothesis and takes the tested BR($t \to bH^+$) into account. Effectively, this brings the signal+background expectation closer to the background-only expectation.

The following procedure is applied:

1. Apply the τ+jets event selection to embedded events to obtain the m_{T} shape.
2. From collision data, count the number of events in the m_{T} distribution between $0 - 40$ GeV after subtracting the background from objects misidentified as τ jets.
3. Using this number, normalize the m_{T} distribution from embedded events using the ratio of events in collision data and embedded data.

For technical reasons, the trigger simulation cannot be re-run for embedded events. As the number of events entering the embedding control sample and passing the whole event selection is still relatively small, the event selection applied to the embedded events is modified by requiring a τ identified using loose criteria. This can be done because the m_{T} distribution is normalized to data and, as Fig. 7 (left) shows, the looser cuts do not bias the shape significantly.

The result is shown in Fig. 7 (right). As can be seen, the uncertainty of the background estimate is currently limited by the statistical uncertainty due to the limited number of events in the $t\bar{t}$ control sample. In the range $40 < m_{\mathrm{T}} < 300$ GeV, there are 21 ± 5 background events with true τ jets expected where the uncertainty is due to the limited number of events in the control sample, and of the data in the region to which the shape is normalized to. In data, 26 events are observed after subtracting the background predicted by the misidentification probability methods and the multi-jet estimate. Within statistical uncertainties, the background prediction and data agree well.

5.3.3 Systematic uncertainties

The following systematic uncertainties are associated with the background prediction:

- To study the effect of additional multi-jet background on the embedding and the control sample selection itself, the μ isolation requirement is varied. To study a potential bias introduced by the embedding method parameters chosen, alternative values are used for the inner and outer cone size in which calorimeter cell depositions are replaced or added. To account for the fact that a small amount of pile-up-related activity can be present in the calorimeter cells removed in a cone around the muon, the effect of only removing half of this energy before adding the τ jet is studied. This results in a systematic uncertainty of 7% on the background normalisation.
- The systematic uncertainty due to the difference in the m_{T} shape as a consequence of loosening the selection with respect to the H^+ selection, as shown in Fig. 7, results in a 8% uncertainty on the background normalisation, and a shift of about 2 GeV in the m_{T} distribution.
- The impact of the incomplete treatment of the τ polarisation in embedded events results in an uncertainty on the m_{T} shape which is estimated by comparing bin by bin the difference in the number of events for simulated $t\bar{t}$ events with and without correct treatment of the τ polarisation.

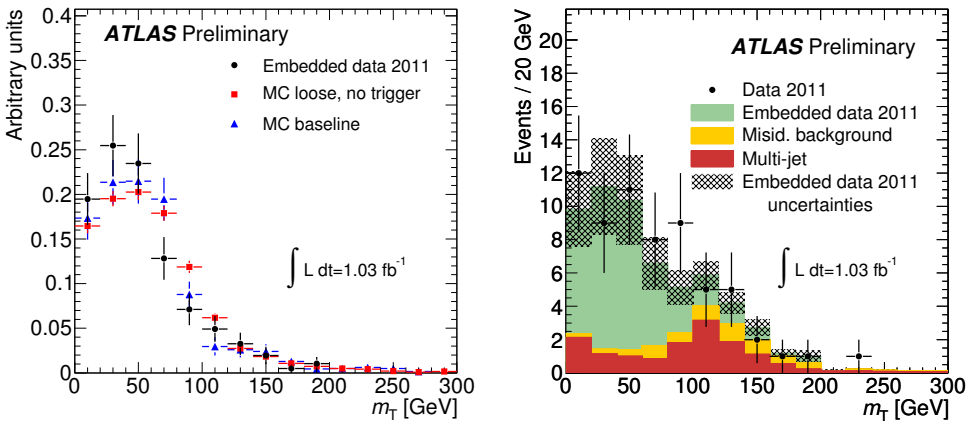

Figure 7: Left: Comparison of the m_{T} shape for simulation and for embedded events (with loose τ identification) used to estimate the background with true τ jets. The distribution from simulation is shown both after the H^+ baseline selection and after the same selection but without trigger requirement and loose τ identification. All distributions are normalized to unit area. Right: Comparison of the m_{T} shape for embedded events versus collision data. The prediction using the embedding method is stacked on top of the expected backgrounds with objects misidentified as τ jets: MC expectation for $t\bar{t}$ and electroweak processes, and the data-driven estimate for multi-jet events. The comparison is done after the H^+ event selection and after normalizing the m_{T} distribution of embedded events to the data distribution in the range 0 – 40 GeV. The gray area indicates the size of the statistical and systematic uncertainties of the embedding method estimate.

This results in an uncertainty on the normalisation of 15%, and the m_{T} distribution is shifted by about 7 GeV which corresponds to 14% of the average m_{T}.

- The impact on the m_{T} distribution due to the uncertainty on the τ energy scale (Table 2) is evaluated, leading to a normalisation uncertainty of $+4/-2\%$, and a shift in the m_{T} distribution by ± 1 GeV.

The statistical uncertainty of the estimate is 8% due to the limited size of the control sample, and additionally 20% due to the normalisation to data (allowing data to fluctuate within one standard deviation for $m_{\mathrm{T}} < 40$ GeV). The numbers above are only indicative, for the limit calculation the full shape uncertainty is used.

6 Results

The results of the data-driven methods in estimating the contributions of the various categories of backgrounds after the baseline selection are summarized in Table 5, and the m_{T} distribution of the remaining events is shown in Fig. 8. The total systematic uncertainty on the background prediction is about 30% but can reach up to 70% for $m_{\mathrm{T}} > 100$ GeV. For the signal, the total systematic uncertainty on the yield is about 40% with a small dependence on m_{H^+}. The number of events with true τ jets has been estimated with the embedding method, the jet $\rightarrow \tau$ misidentification events with intrinsic $E_{\mathrm{T}}^{\mathrm{miss}}$ with γ+jets control samples, the $e \rightarrow \tau$ misidentification events with $Z/\gamma^* \rightarrow ee$ control samples, and the multi-jet contribution by taking its shape from a sideband region and fitting it to the data. The number of events with $m_{\mathrm{T}} > 40$ GeV is given which allows for a better comparison of data and expectation as the estimate from the embedding method is normalized to data in the range $m_{\mathrm{T}} < 40$ GeV. A good agreement between the estimated and the observed number of events is seen.

Table 5: Expected number of events from data-driven estimates with $m_{\mathrm{T}} > 40$ GeV, and as observed in data. Only statistical uncertainties are given.

	Events with/from					
	true τ jets	jet $\rightarrow \tau$ mis-id	$e \rightarrow \tau$ mis-id	multi-jet	expected (sum)	data
$m_{\mathrm{T}} > 40$ GeV	21 ± 5	2.4 ± 0.7	1.9 ± 0.2	12 ± 5	37 ± 7	43

Using data-driven background estimates, no statistically significant excess of events is observed in 1.03 fb^{-1} of collision data. Exclusion limits are set on the branching ratio $t \rightarrow bH^+$, and in the $m_{H^+} - \tan\beta$ plane, by rejecting the signal hypothesis at the 95% confidence level applying the CL$_s$ procedure [42, 43]. A profile likelihood ratio [44] is used with the m_{T} distribution as the discriminating variable. The statistical analysis is based on a binned likelihood function for the m_{T} distribution. Systematic uncertainties in shape and normalisation are incorporated via nuisance parameters and the one-sided profile likelihood ratio, $\tilde{q}_\mu$, is used as a test statistic. The final limits are based on the asymptotic distribution of the test statistic [44].

The resulting exclusion limit is shown in Fig. 9 in terms of $\mathrm{BR}(t \rightarrow H^+b) \times \mathrm{BR}(H^+ \rightarrow \tau^+\nu)$. Figure 10 shows the upper limit in the context of the m_h^{max} scenario of the MSSM [45] in the m_{H^+}-$\tan\beta$ plane. No exclusion limit is shown for charged Higgs boson masses close to 160 GeV as no reliable calculations for $\mathrm{BR}(t \rightarrow H^+b)$ exist for $\tan\beta$ values in the range of interest. The following relative uncertainties on $\mathrm{BR}(t \rightarrow bH^+)$ are considered [46]: 5% for one-loop electro-weak corrections missing in the calculations, 2% for missing two-loop QCD corrections, and about 1% (depending on $\tan\beta$) Δ_b-induced uncertainties (where Δ_b is a correction factor to the running bottom quark mass [47]). These

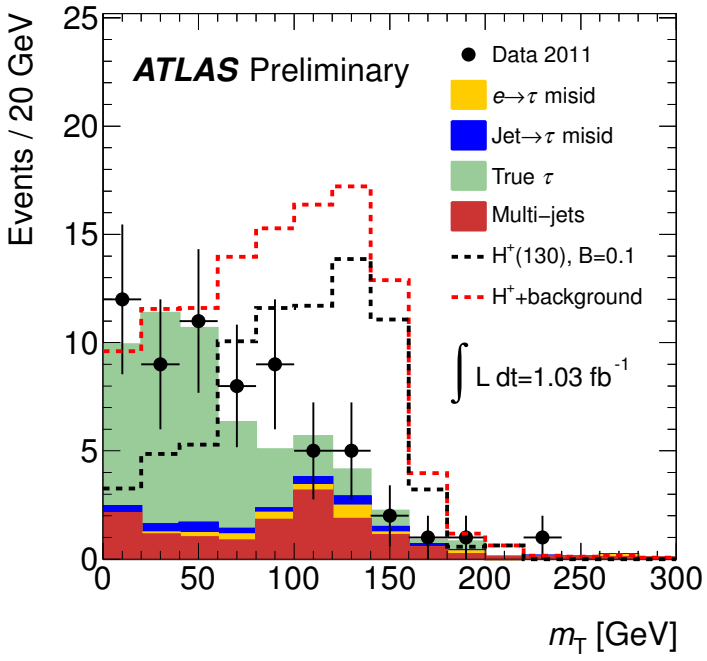

Figure 8: The m_{T} distribution after event selection. The observation in collision data, and the estimates from data-driven methods are compared. The distribution of the H^+ signal is given for a reference point in parameter space corresponding to $\mathrm{BR}(t \to bH^+) = 10\%$, thus the SM-like $t\bar{t}$ background is reduced correspondingly.

uncertainties are added linearly. This result constitutes a significant improvement compared to existing limits provided by the Tevatron experiments [6] over the whole investigated mass range, but in particular for charged Higgs boson masses close to the top quark mass.

7 Conclusions

Charged Higgs bosons are searched for in the decay mode $t \to bH^+$, $H^+ \to \tau\nu$, with hadronically decaying τ leptons, using $t\bar{t}$ events reconstructed in a total of 1.03 fb^{-1} of $\sqrt{s} = 7$ TeV pp collision data recorded with the ATLAS experiment. Data-driven methods, employed to estimate the number of background events characterized by the presence of a τ jet, $E_{\mathrm{T}}^{\mathrm{miss}}$, b jets, and a hadronically decaying W boson, predict 37 ± 7(stat) events with $m_{\mathrm{T}} > 40$ GeV. A total of 43 such events are observed which is consistent with the prediction. The CL_s procedure is used to derive 95% CL exclusion limits. Values of the product of branching ratios, $\mathrm{BR}(t \to bH^+) \times \mathrm{BR}(H^+ \to \tau^+\nu)$, larger than 0.03 – 0.10 have been excluded in the H^+ mass range 90 – 160 GeV, significantly extending limits from other experiments. Interpreted in the context of the m_h^{max} scenario of the MSSM, values of $\tan\beta$ above 22 – 30 (depending on m_{H^+}) can be excluded in the mass range 90 GeV $< m_{H^\pm} <$ 140 GeV.

References

[1] J. F. Gunion, H. E. Haber, G. Kane, and S. Dawson, *The Higgs Hunter's Guide*. Addison-Wesley, 1990.

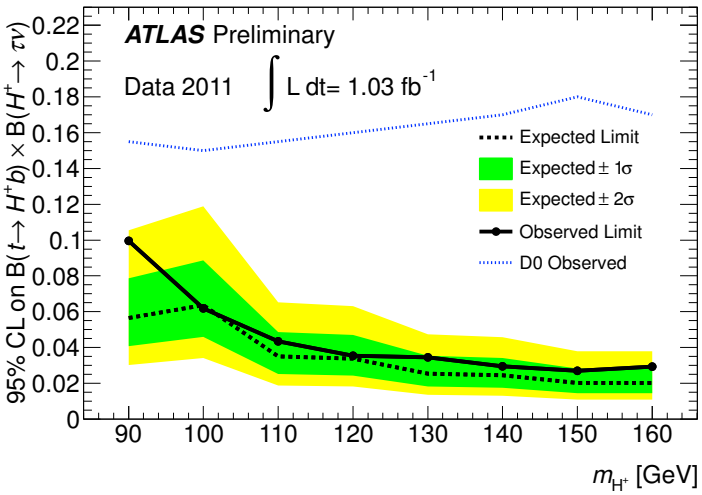

Figure 9: Expected and observed 95% CL exclusion limits for charged Higgs boson production from top quark decays as a function of m_{H^+} in terms of BR($t \to H^+b$) $\times$ BR($H^+ \to \tau^+\nu$). For comparison, the best limit provided by the Tevatron experiments is shown [6].

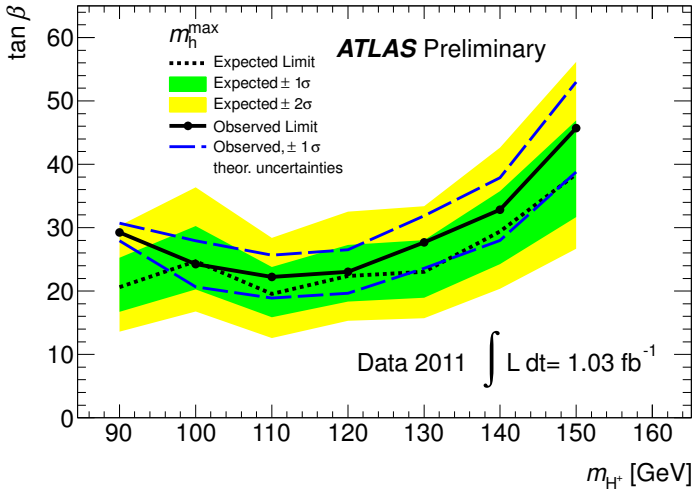

Figure 10: Limit for charged Higgs boson production from top quark decays in the m_{H^+}-tanβ plane. Results are shown for the MSSM scenario $m_h^{\max}$.

[2] J. F. Gunion, H. E. Haber, G. L. Kane, and S. Dawson, *Errata for "The Higgs Hunter's Guide"*, hep-ph/9302272.

[3] J. F. Gunion and H. E. Haber, *Higgs Bosons in Supersymmetric Models. 1.*, Nucl.Phys. **B272** (1986) 1.

[4] K. Inoue, A. Kakuto, H. Komatsu, and S. Takeshita, *Aspects of Grand Unified Models with Softly Broken Supersymmetry*, Prog. Theor. Phys. **68** (1982) 927.

[5] LHC Higgs Cross Section Working Group Collaboration, S. Dittmaier et al., *Handbook of LHC Higgs Cross Sections: 1. Inclusive Observables*, arXiv:1101.0593 [hep-ph].

[6] D0 Collaboration, V. M. Abazov et al., *Search for charged Higgs bosons in top quark decays*, Phys. Lett. **B682** (2009) 278–286, arXiv:0908.1811 [hep-ex].

[7] LEP Higgs Working Group for Higgs boson searches Collaboration, *Search for charged Higgs bosons: Preliminary combined results using LEP data collected at energies up to 209 GeV*, arXiv:hep-ex/0107031.

[8] CMS Collaboration, *$H^+ \to \tau$ in Top quark decays*, CMS-PAS-HIG-11-008 (2011) .

[9] ATLAS Collaboration, *The ATLAS Experiment at the CERN Large Hadron Collider*, JINST **3** (2008) S08003.

[10] S. Frixione and B. R. Webber, *Matching NLO QCD computations and parton shower simulations*, JHEP **0206** (2002) 029, arXiv:hep-ph/0204244 [hep-ph].

[11] G. Corcella, I. Knowles, G. Marchesini, S. Moretti, K. Odagiri, et al., *HERWIG 6: An Event generator for hadron emission reactions with interfering gluons (including supersymmetric processes)*, JHEP **0101** (2001) 010, arXiv:hep-ph/0011363 [hep-ph].

[12] J. Butterworth, J. R. Forshaw, and M. Seymour, *Multiparton interactions in photoproduction at HERA*, Z.Phys. **C72** (1996) 637–646, arXiv:hep-ph/9601371 [hep-ph].

[13] S. Frixione, E. Laenen, P. Motylinski, and B. R. Webber, *Single-top production in MC@NLO*, JHEP **0603** (2006) 092, arXiv:hep-ph/0512250 [hep-ph].

[14] ATLAS Collaboration, *Measurement of the top quark-pair production cross section with ATLAS in pp collisions at $\sqrt{s}$ = 7 TeV*, arXiv:1012.1792 [hep-ex].

[15] U. Langenfeld, S. Moch, and P. Uwer, *New results for $t\bar{t}$ production at hadron colliders*, arXiv:0907.2527 [hep-ph].

[16] M. L. Mangano, M. Moretti, F. Piccinini, R. Pittau, and A. D. Polosa, *ALPGEN, a generator for hard multiparton processes in hadronic collisions*, JHEP **0307** (2003) 001, arXiv:hep-ph/0206293 [hep-ph].

[17] R. Gavin, Y. Li, F. Petriello, and S. Quackenbush, *FEWZ 2.0: A code for hadronic Z production at next-to- next-to-leading order*, Comput. Phys. Commun. **182** (2011) 2388–2403, arXiv:1011.3540 [hep-ph].

[18] T. Sjostrand, S. Mrenna, and P. Z. Skands, *PYTHIA 6.4 Physics and Manual*, JHEP **0605** (2006) 026, arXiv:hep-ph/0603175 [hep-ph].

[19] Z. Was and P. Golonka, *TAUOLA as tau Monte Carlo for future applications*, Nucl.Phys.Proc.Suppl. **144** (2005) 88–94, arXiv:hep-ph/0411377 [hep-ph].

[20] E. Barberio, B. van Eijk, and Z. Was, *PHOTOS: A Universal Monte Carlo for QED radiative corrections in decays*, Comput. Phys. Commun. **66** (1991) 115–128.

[21] ATLAS Collaboration, *Charged particle multiplicities in pp interactions at $\sqrt{s}$ = 0.9 and 7 TeV in a diffractive limited phase-space measured with the ATLAS detector at the LHC and new PYTHIA6 tune*, ATLAS-CONF-2010-031 (2010) .

[22] ATLAS Collaboration, *First tuning of HERWIG/JIMMY to ATLAS data*, ATL-PHYS-PUB-2010-014 .

[23] GEANT4 Collaboration, S. Agostinelli et al., *GEANT4: A simulation toolkit*, Nucl. Instrum. Meth. **A506** (2003) 250–303.

[24] ATLAS Collaboration, *The ATLAS Simulation Infrastructure*, Eur.Phys.J. **C70** (2010) 823–874, arXiv:1005.4568 [physics.ins-det].

[25] ATLAS Collaboration, *Data-Quality Requirements and Event Cleaning for Jets and Missing Transverse Energy Reconstruction with the ATLAS Detector in Proton-Proton Collisions at a Center-of-Mass Energy of $\sqrt{s}$ = 7 TeV*, ATLAS-CONF-2010-038 (2010) .

[26] M. Cacciari, G. P. Salam, and G. Soyez, *The Anti-k(t) jet clustering algorithm*, JHEP **0804** (2008) 063, arXiv:0802.1189 [hep-ph].

[27] M. Cacciari and G. P. Salam, *Dispelling the N**3 myth for the k(t) jet-finder*, Phys.Lett. **B641** (2006) 57–61, arXiv:hep-ph/0512210 [hep-ph].

[28] W. Lampl et al., *Calorimeter clustering algorithms: Description and performance*, ATL-LARG-PUB-2008-002 (2008) .

[29] ATLAS Collaboration, *Jet energy scale and its systematic uncertainty in proton-proton collisions at sqrt(s)=7 TeV in ATLAS 2010 data*, ATLAS-CONF-2011-032 (2011) .

[30] ATLAS Collaboration, *Commissioning of the ATLAS high-performance b-tagging algorithms in the 7 TeV collision data*, ATLAS-CONF-2011-102 (2011) .

[31] ATLAS Collaboration, *Reconstruction, Energy Calibration, and Identification of Hadronically Decaying Tau Leptons in the ATLAS Experiment*, ATLAS-CONF-2011-077 (2011) .

[32] ATLAS Collaboration, *Measurement of the $W \to \ell\nu$ and $Z/\gamma^* \to \ell\ell$ production cross sections in proton-proton collisions at $\sqrt{s}$ = 7 TeV with the ATLAS detector*, JHEP **12** (2010) 060, arXiv:1010.2130 [hep-ex].

[33] ATLAS Collaboration, *Expected electron performance in the ATLAS experiment*, ATLAS-PHYS-PUB-2011-006 (2011) .

[34] ATLAS Collaboration, *Muon reconstruction efficiency in reprocessed 2010 LHC p-p collision data recorded with the ATLAS detector*, ATLAS-CONF-2011-063 (2011) .

[35] ATLAS Collaboration, *CERN-OPEN-2008-020*, arXiv:0901.0512.

[36] ATLAS Collaboration, *Luminosity Determination in pp Collisions at sqrt(s) = 7 TeV using the ATLAS Detector in 2011*, ATLAS-CONF-2011-116 (2011) .

[37] D. Casadei et al., *The implementation of the ATLAS missing Et triggers for the initial LHC operation*, ATL-DAQ-PUB-2011-001 (2011) .

[38] ATLAS Collaboration, *Performance of the ATLAS tau trigger in p-p collisions at* $\sqrt{s} = 7$ *TeV*, ATLAS-CONF-2010-090 (2010) .

[39] ATLAS Collaboration, *Measurement of the Mis-identification Probability of Tau Leptons from Hadronic Jets and from Electrons*, ATLAS-CONF-2011-113 (2011) .

[40] ATLAS Collaboration, *Expected photon performance in the ATLAS experiment*, ATLAS-PHYS-PUB-2011-007 (2011) .

[41] ATLAS Collaboration, *Data-driven estimation of the background to charged Higgs boson searches using hadronically-decaying tau final states in ATLAS*, ATLAS-CONF-2011-051 (2011) .

[42] A. L. Read, *Presentation of search results: the CL s technique*, Journal of Physics G: Nuclear and Particle Physics **28** (2002) no. 10, 2693.

[43] T. Junk, *Confidence Level Computation for Combining Searches with Small Statistics*, Nucl. Instrum. Meth. **434** (1999) 435.

[44] G. Cowan, K. Cranmer, E. Gross, and O. Vitells, *Asymptotic formulae for likelihood-based tests of new physics*, Eur.Phys.J. **C71** (2011) 1554, arXiv:1007.1727 [physics.data-an].

[45] M. S. Carena, S. Heinemeyer, C. E. M. Wagner, and G. Weiglein, *Suggestions for benchmark scenarios for MSSM Higgs boson searches at hadron colliders*, Eur. Phys. J. **C26** (2003) 601–607, arXiv:hep-ph/0202167.

[46] LHC Higgs Cross Section Working Group Collaboration, S. Dittmaier et al., *Handbook of LHC Higgs Cross Sections: 2. Differential Distributions*, .

[47] M. S. Carena, D. Garcia, U. Nierste, and C. E. M. Wagner, *Effective Lagrangian for the* $\bar{t}bH^+$ *interaction in the MSSM and charged Higgs phenomenology*, Nucl. Phys. **B577** (2000) 88–120, arXiv:hep-ph/9912516.

[48] G. Cowan, K. Cranmer, E. Gross, and O. Vitells, *Power-Constrained Limits*, arXiv:1105.3166 [physics.data-an].

A Limit figure with PCL

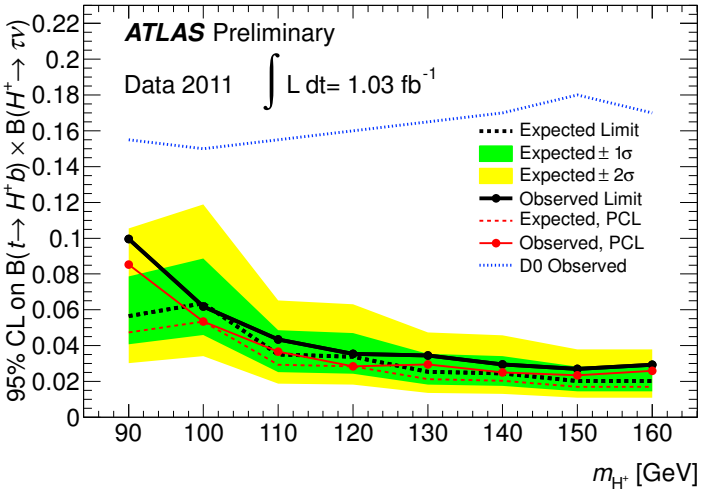

Figure 11: Expected and observed 95% CL exclusion limits for charged Higgs boson production from top quark decays as a function of m_{H^+} in terms of BR($t \to H^+b$) $\times$ BR($H^+ \to \tau^+\nu$) using the CL$_s$ procedure. Power-Constrained limits (PCL) [48] with a 50% power constraint are shown as well. For comparison, the best limit provided by the Tevatron experiments is shown [6].